Accepted Manuscript

Synthesis, biological evaluation and 3D-QSAR studies of novel 5-phenyl-1*H*-pyrazol cinnamamide derivatives as novel antitubulin agents

Shu-Fu Wang, Yong Yin, Ya-Liang Zhang, Shan-Wei Mi, Meng-Yue Zhao, Peng-Cheng Lv, Bao-Zhong Wang, Hai-Liang Zhu

PII: S0223-5234(15)00114-2

DOI: 10.1016/j.ejmech.2015.02.018

Reference: EJMECH 7700

To appear in: *European Journal of Medicinal Chemistry*

Received Date: 26 October 2014

Revised Date: 8 February 2015

Accepted Date: 12 February 2015

Please cite this article as: S.-F. Wang, Y. Yin, Y.-L. Zhang, S.-W. Mi, M.-Y. Zhao, P.-C. Lv, B.-Z. Wang, H.-L. Zhu, Synthesis, biological evaluation and 3D-QSAR studies of novel 5-phenyl-1*H*-pyrazol cinnamamide derivatives as novel antitubulin agents, *European Journal of Medicinal Chemistry* (2015), doi: 10.1016/j.ejmech.2015.02.018.

Synthesis, biological evaluation and 3D-QSAR studies of novel 5-phenyl-1*H*-pyrazol cinnamamide derivatives as novel antitubulin agents

Shu-Fu Wang [+], *Yong Yin* [+], *Ya-Liang Zhang, Shan-Wei Mi, Meng-Yue Zhao, Peng-Cheng Lv*, Bao-Zhong Wang*, Hai-Liang Zhu**

State Key Laboratory of Pharmaceutical Biotechnology, Nanjing University, Nanjing 210093, People's Republic of China

[+] *These authors contributed equally to this work.*

[*] *Corresponding authors. Tel.: +86 25 83592572; Fax: +86 25 83592672.*

E-mail address: zhuhl@nju.edu.cn (H.-L. Zhu).

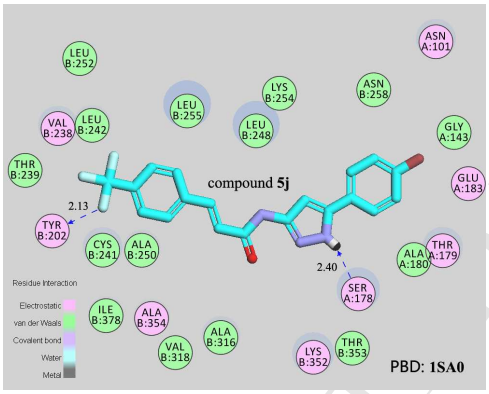

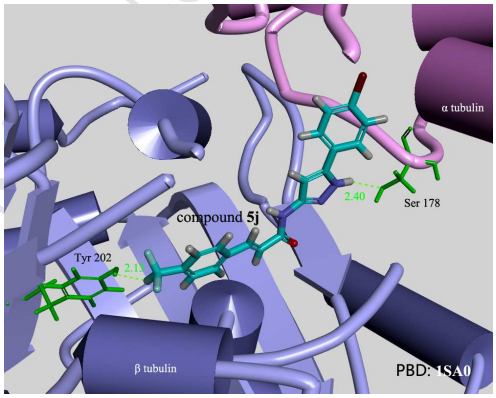

Compound **5j** exhibited the most potent inhibitory activity with an IC_{50} value of 1.02 μM for tubulin, 0.35 μM for MCF-7, 0.62 μM for A549 and 0.57μM for B16-F10.

Synthesis, biological evaluation and 3D-QSAR studies of novel 5-phenyl-1*H*-pyrazol cinnamamide derivatives as novel antitubulin agents

Shu-Fu Wang [+], *Yong Yin* [+], *Ya-Liang Zhang, Shan-Wei Mi, Meng-Yue Zhao, Peng-Cheng Lv*, Bao-Zhong Wang*, Hai-Liang Zhu**

State Key Laboratory of Pharmaceutical Biotechnology, Nanjing University, Nanjing 210093, People's Republic of China

[+] These authors contributed equally to this work.

Abstract

A series of novel 5-phenyl-1*H*-pyrazol derivatives (**5a**-**5x**) containing cinnamamide moiety were synthesized and their biological activities as potential tubulin polymerization inhibitors were evaluated. Among them, compound **5j** exhibited the most potent inhibitory activity with an IC_{50} value of 1.02 μM for tubulin, which was superior to that of Colchicine (IC_{50} = 1.34 μM). Docking simulation was performed to insert compound **5j** into the crystal structure of tubulin at colchicine binding site to determine the probable binding model. 3D-QSAR model was also built to provide more pharmacophore understanding that could be used to design new agents with more potent tubulin inhibitory activity.

Keywords: Pyrazole; Cinnamamide; Antitubulin agent; Molecular docking; 3D-QSAR

Abbreviations: SAR, structure-activity relationship; IC_{50}, half maximal inhibitory concentration; MTT, 3-(4, 5-Dimethylthiazol-2-yl)-2,5-diphenyltetrazolium bromide

[*] Corresponding authors. Tel.: +86 25 83592572; Fax: +86 25 83592672.

E-mail address: zhuhl@nju.edu.cn

1. Introduction

Microtubules are major cytoskeletal protein polymers in all eukaryotic cells and involved in numerous cellular functions including chromosome segregation, intracellular transport, cell motility, and cell shape.[1] Microtubules assemble and disassemble by a reversible process involving discrete α/β tubulin heterodimers. This dynamic instability feature along with treadmilling gives microtubules significant role in mitosis and cell division.[2] During cell mitosis, microtubules mediate the timely and correct attachment of chromosomes at their kinetochores to the spindle, the complex movements of the chromosomes that bring them to their properly aligned positions and the synchronous separation of the chromosomes.[3] Given the importance of microtubules in cell mitosis, microtubules or tubulins serve as effected molecular targets for cancer chemotherapeutic agents.

There are two classes of these chemotherapeutic agents, microtubule stabilizers (e.g., paclitaxel and docetaxel), and microtubule destabilizers (e.g., vinblastine and vincristine). Both types interfere with the mitotic spindle assembly during cell division and block cell cycle in G2/M phases, resulting in cell death.[4-6] Colchicine (Figure 1) is the first identified antimitotic drug that inhibits microtubule polymerization by binding to tubulin, and its binding site has been well characterized.[7] Several other new compounds such as E7010, HMN-214, and CA-4 (Figure 1) have also attracted much interest as antitubulin agents. They bound tubulins through colchicine binding site.[8]

Chalcones are the biogenetic precursors of all known flavonoids and exhibit a variety of biological activities including anticancer,[9-11] anti-inflammatory,[12.13] anti-tuberculosis,[12] anti-fungal and antiproliferative activities.[14-22] Antimitotic agents like *trans*-1-(2,5-dimethoxy)-3-[4 (dimethylamino) phenyl]-2-methyl-2-propen-1-one (**MDL**) possess a chalcone skeleton and display rapid and reversible binding to the colchicine binding site of β-tubulin at the interface with α-tubulin and cause inhibition of its assembly to microtubules.[23] Researches showed that their broad biological properties are largely due to the α, β-unsaturated ketone moiety.[24]

As shown in Figure 2, chalcone and cinnamon amide share similar part of the active structure. Cinnamic acids are abundant in various natural resources and its natural analogues are unique as anticancer agents.[25] A lot of cinnamido compounds were also synthesized and their anticancer abilities were evaluated by our research groups.[26-28] Besides, Pyrazole-based heterocycles play a crucial role in the arena of rigidified combretastatin analogues.[29] Lee and co-workers described a series of 3,5-diarylpyrazoles that display low cytotoxicity in tumor cell lines due to their planar conformation.[30] These previous researches encouraged us to integrate cinnamon amide with pyrazoles to screen compounds which have potent anticancer activities.

Herein we report the synthesis and bioactivities of a series of 5-phenyl-1*H*-pyrazol derivatives containing cinnamoyl moiety. Biological evaluation indicated that some of the synthesized compounds were potent inhibitors of tubulin. Docking simulation was performed using the X-ray crystallographic structure of tubulin to explore the binding mode of the compound at the active site.

2. Results and discussion

2.1. Chemistry

The synthetic route of the pyrazol derivatives(**5a-5x**) was outlined in Scheme 1. First of all, **2a-2c** were synthesized in THF by treating *p*-substituted benzoate with acetonitrile using NaH as catalyst. Secondly, compounds **2a-2c** and hydrazine hydrate were dissolved in ethanol and refluxed for 1 h to get compounds **3a-3c**. Lastly, the coupling reaction between the obtained compounds **3a-3c** and nicotinic acids was performed by using 1-ethyl-3-(3-dimethylaminopropyl) carbodiimide hydrochloride (EDCl) and N-hydroxybenzotriazole (HOBt) in anhydrous methylene dichloride, and refluxed to give the desired compounds **5a-5x**. All of the synthesized compounds were given satisfactory analytical and spectroscopic data, which were in full accordance with their depicted structures.

2.2. Antiproliferative effects against cancer cells

To test the anticancer activities of the synthesized compounds, we evaluated antiproliferative activities of compounds **5a-5x** against MCF-7, A549 and B16-F10

cancer cells. The results were summarized in Table 1. These 5-phenyl-1*H*-pyrazol derivatives bearing cinnamoyl moiety displayed remarkable antiproliferative effects.

The results demonstrated that a *p*-substituted electron-withdrawing or halogen group on phenyl ring A may have slightly improved antiproliferative activities in the order 4-CF_3＞4-NO_2＞4-OMe＞4-F＞4-Cl＞4-Br＞H>4-Me. In the case of constant A ring substituents, change of substituents on B-ring could also affect the activities of compounds and the inhibitory activities of compounds with different substituents on ring B. The activities increased in the following order: 4-Me<H<4-Br, suggesting that an electron-withdrawing could enhance the competence of the pyrazol derivatives.

2.3. Tubulin polymerization inhibition

To examine whether the compounds interact with tubulin and inhibit tubulin polymerization in vitro, we performed the abilities of the synthesized compounds in inhibiting the polymerization of tubulin. The IC_{50} of the compounds were summarized in Table 2. It was observed that all the synthesized compounds showed inhibitory activities of tubulin displaying IC_{50} values between 1.02 and 3.36 μM. Among them, compound **5j** displayed the most potent anti-tubulin polymerization activity with IC_{50} of 1.02 μM.

2.4. Effects on cell cycle against cancer cells

To gain further insight into the action mode of these compounds, the most potent one was further assayed for its effects on cell cycle using flow cytometry (Figure 3). As is shown in Figure 3, compound **5j** strongly induced G2/M arrest in MCF-7 cells, and the effect was observed in a dose-independent manner after treatment with increasing dose of the compound. About 45.45% of the cells were arrested in the G2/M phase while 76.95% of the cells were found to be in the G2/M phase after treatment with **5j** of 1 and 2 μg/mL for 24 h, respectively. These findings indicated a continuing impairment of cell division and confirmed compound **5j** was a potent antitubulin agent.

2.5. Molecular docking study

To gain better understanding on the potency of the synthesized compounds and guide further SAR studies, we proceeded to examine the interaction of the 5-phenyl-1*H*-pyrazol derivatives with tubulin (PDB code: 1SA0). The molecular docking was performed by inserting synthetic compounds into the colchicine binding site in tubulin. All docking runs were applied LigandFit Dock protocol of Discovery Studio 3.5. The binding model of compound **5j** and tubulin was depicted in Figure 4. and the enzyme surface model was shown in Figure 5, which revealed that the molecule is well filled in the active pocket.

In the binding mode, compound **5j** is nicely bound to tubulin via two hydrogen bonds. The hydrogen atom on the pyrazole ring with the oxygen atom on the main chain of Ser178 (angle N-H···O = 160.6°, distance = 2.40 Å) and the fluorine atom of CF_3 with the hydrogen atom on the hydroxy of Tyr202 (angle F···H-O = 113.3°, distance = 2.13 Å) contribute to the hydrogen bonding interaction together, being a probable explanation for its nice activity. Meanwhile, the receptor surface model showed in Figure 5 revealed that this candidate inhibitor was tightly embedded into the active pocket of tubulin. This molecular docking result, along with the enzyme assay data, suggested that compound **5j** is a potential inhibitor of tubulin.

2.6. 3D-QSAR

In order to acquire a systematic SAR profile on the synthesized compounds and to explore the more powerful and selective tubulin inhibitors, 3D-QSAR model was built to choose activity conformation of the designed molecular and reasonably evaluated the designed molecules by using the corresponding pIC_{50} values which were converted from the obtained IC_{50} (μM) values of tubulin inhibition and performed by built-in QSAR software of DS 3.5 (Discovery Studio 3.5, Accelrys, Co. Ltd). By convention, the pIC_{50} scale ($-\log IC_{50}$), in which higher values indicate exponentially greater potency, is used as a method to measure inhibitory activity. The training and test set was chosen by the Diverse Molecules method in Discovery Studio. Considering a good alignment is very important for the analysis of molecular

fields, we applied CDOCKER protocol to explore each molecule with lowest energy before alignment conformation. 5-phenyl-1*H*-pyrazol was selected as substructure to build alignment conformation before building the QSAR model.

The correlation coefficient r^2 between observed and predicted activity of training set was found to be 0.991, while that of test set was found to be 0.796, which proved that the QSAR model built by us was acceptable. The q^2 of 5-fold cross validation result is 0.603 while the q^2 of validation result using external test set is 0.796. It means that the model performs well with compounds aligned by docking and the predictive ability of our QSAR model is acceptable. Predicted pIC_{50} values and residual errors of 24 compounds by this QSAR model had been given in Table 3. The well agreement between predicted pIC_{50} value and experimental pIC_{50} value for both test sets and training sets are shown in Figure 6.

Also the molecules aligned with the iso-surfaces of the 3D-QSAR model coefficients on electrostatic potential grids (Figure 7a) and van der Waals grids (Figure 7b) are listed. Electrostatic map indicates red contours around regions where high electron density (negative charge) is expected to increase activity, and blue contours represent areas where low electron density (partial positive charge) is expected to increase activity. Similarly, steric map indicates areas where steric bulk is predicted to increase (green) or decrease (yellow) activity.

According to the maps, it was suggested that the compound with high negative charged and bulky R_2 group would show higher activity, validating that CF_3 substituted group being a better choice than mono fluorine substituted group and F substituent better than Cl as well as Cl substituent better than Br. Meanwhile, we can get from the maps that compound with high negative charged R_1 group would show better activity than compound with low negative charged R_1 group, validating that Br substituent better than H and CH_3. As a result, data summarized above demonstrated that compounds **5j**, the most potent tubulin inhibitor (IC_{50} = 1.02 μM), which contains suitable substituents, had an outstanding activity.

3. Conclusion

In this paper, a series of novel tubulin inhibitors beared pyrazole core and cinnamamide moiety have been synthesized and their biological activities were evaluated. Among them, compound **5j** exhibited the most potent tubulin inhibition activities (IC_{50} = 1.02 μM for tubulin) and antiproliferative activities (IC_{50} = 0.35 μM for MCF-7, IC_{50} = 0.62 μM for A549 and IC_{50} = 0.57 μM for B16-F10). Docking simulation was performed to put compound **5j** into the colchicine binding site of tubulin to determine the potential binding model and found that several interactions with the protein residues in the colchicine binding site might play an important role in its antitubulin polymerization and antiproliferative activities. QSAR model was built to provide a reliable tool for reasonable design of novel tubulin inhibitors in future.

4. Experiments

4.1. Materials and measurements

All chemicals and reagents used in current study were analytical grade. The reactions were monitored by glass-backed silica gel sheets (Silica Gel 60 GF254). Column chromatography was performed using silica gel (200–300 mesh) eluting with ethyl acetate and petroleum ether. Melting points (uncorrected) were determined on a XT4MP apparatus (Taike Corp., Beijing, China). ESI mass spectra were obtained on a Mariner System 5304 mass spectrometer, and ^{1}H NMR spectra were collected on a Bruker DPX400 or DPX300 model spectrometer at room temperature with TMS and solvent signals allotted as internal standards. The solvent signals allotted as internal stands. Elemental analyses were performed on a CHN-O-Rapid instrument. All the compounds gave satisfactory chemical analyses (±0.4%).

4.2. General procedure for the synthesis of 2a-2c

Mixed *p*-substituted methyl benzoate (7 mmol) with NaH (14 mmol, 0.35 g) in boiling tetrahydrofuran (5 mL) and then followed by dropwise addition of solution of acetonitrile (7 mmol, 0.29g, 0.4 mL) in tetrahydrofuran (1 mL). The resulting mixture was refluxed for 4 h and then cooling down to room temperature, after which the

solution was diluted with diethylether (15 mL) and left to stand at room temperature for 48 h. The precipitated sodium salt was filtered and washed with diethylether. The dry compound was dissolved in water (5 mL) and acidified with HCl (1mol/L) to pH 2. The collected extracts were crystallized from toluene, filtered and dried with Na_2SO_4.

4.3. General procedure for the synthesis of 3a-3c

To a stirred mixture of compound **2a-2c** (5 mmol) in EtOH (25 mL) were added $NH_2NH_2 \cdot H_2O$ (0.3 mL, 6 mmol) and CH_3SO_3H (0.1 mL, 1 mmol) at room temperature and the mixture was stirred under reflux for 1h. The precipitate was purified by column chromatograghy over silica gel to give the compound **3a-3c**.

4.4.General procedure for the synthesis of 5-phenyl-1*H*-pyrazol derivatives (5a-5x)

Compounds **5a-5x** were synthesized by coupling substituted **3a-3c** with cinnamic acids, using 1-ethyl-3-(3-dimethylaminopropyl) carbodiimide hydrochloride (EDCl) and *N*-hydroxybenzotriazole (HOBt) as condensing agent. The mixture was refluxed in anhydrous CH_2Cl_2 for 1-3 h. The products were extracted with ethyl acetate. The extract was washed successively with 5% HCl, then evaporated and purified by column chromatograghy over silica gel to give the compound.

4.4.1 (*E*)-3-(4-nitrophenyl)-*N*-(5-phenyl-1*H*-pyrazol-3-yl)acrylamide(5a)

Yellow powder, yield: 74%. m.p. 229-230 °C. 1H NMR (300 MHz, DMSO, δ ppm): 5.90 (s, 1H); 6.88 (s, 2H); 7.46 (m, 3H); 7.97 (m, 3H); 8.14 (m, 3H); 8.32 (d, *J* = 8.32 Hz, 2H). MS (ESI): 335.43 ($[M+H]^+$). Anal. Calcd for $C_{18}H_{14}N_4O_3$: C, 64.66; H, 4.22; N, 16.76%; Found: C, 66.49; H, 4.37; N, 16.51%.

4.4.2 (*Z*)-*N*-(5-phenyl-1*H*-pyrazol-3-yl)-3-(4-(trifluoromethyl)phenyl)acrylamide(5b)

Yellow powder, yield: 69%. m.p. 183-184 °C. 1H NMR (300 MHz, DMSO, δ ppm): 5.89 (s, 1H); 6.87 (s, 2H); 7.43-7.50 (m, 3H); 7.85 (d, *J* = 5.97 Hz, 2H); 7.92-8.00 (m, 3H); 8.07-8.12 (m, 3H). MS (ESI): 358.13 ($[M+H]^+$). Anal. Calcd for

$C_{19}H_{14}F_3N_3O$: C, 63.86; H, 3.95; N, 11.76%; Found: C, 63.63; H, 3.82; N, 11.54%.

4.4.3 *N*-(5-phenyl-1*H*-pyrazol-3-yl)cinnamamide(5c)

Yellow powder, yield: 59%. m.p. 198-199 °C. 1H NMR (300 MHz, DMSO, δ ppm): 5.88 (s, 1H); 6.85 (s, 2H); 7.47 (m, 6H); 7.84-8.02 (m, 6H). MS (ESI): 290.24 ($[M+H]^+$). Anal. Calcd for $C_{18}H_{15}N_3O$: C, 74.72; H, 5.23; N, 14.52%; Found: C, 74.48; H, 5.46; N, 14.37%.

4.4.4 (*E*)-3-(4-methoxyphenyl)-*N*-(5-(p-tolyl)-1*H*-pyrazol-3-yl)acrylamide(5d)

Yellow powder, yield: 69%. m.p. 166-167 °C. 1H NMR (300 MHz, DMSO, δ ppm): 5.88 (s, 1H); 6.84 (s, 2H); 7.34 (t, *J* =13.2, 2H); 7.45 (m, 3H); 7.94 (m, 6H). MS (ESI): 308.53 ([M+H]+). Anal. Calcd for $C_{18}H_{14}FN_3O$: C, 70.35; H, 4.59; N, 13.67%; Found: C, 70.23; H, 4.54; N, 13.34%.

4.4.5 (*E*)-3-(4-chlorophenyl)-*N*-(5-phenyl-1*H*-pyrazol-3-yl)acrylamide(5e)

Yellow powder, yield: 75%. m.p. 185-186 °C. 1H NMR (300 MHz, DMSO, δ ppm): 5.88 (s, 1H); 6.85 (s, 2H); 7.46 (m, 3H); 7.57 (d, *J* = 6.42 Hz, 2H); 7.95 (m, 6H). MS (ESI): 324.78 ($[M+H]^+$). Anal. Calcd for $C_{18}H_{14}ClN_3O$: C, 66.77; H, 4.36; N, 12.98%; Found: C, 66.49; H, 4.55; N, 13.14%.

4.4.6 (*E*)-*N*-(5-phenyl-1*H*-pyrazol-3-yl)-3-(*p*-tolyl)acrylamide(5f)

Yellow powder, yield: 55%. m.p. 189-190 °C. 1H NMR (300 MHz, DMSO, δ ppm): 2.38 (s, 3H); 5.88 (s, 1H); 6.84 (s, 2H); 7.32 (d, *J* = 5.97 Hz, 2H); 7.45 (m, 3H); 7.34 (d, *J* = 6.06 Hz, 2H); 7.92 (m, 4H); MS (ESI): 304.34 ($[M+H]^+$). Anal. Calcd for $C_{19}H_{17}N_3O$: C, 75.23; H, 5.65; N, 13.85%; Found: C, 75.43; H, 5.44; N, 13.74%.

4.4.7 (*Z*)-3-(4-methoxyphenyl)-*N*-(5-phenyl-1*H*-pyrazol-3-yl)acrylamide(5g)

Yellow powder, yield: 69%. m.p. 166-167 °C. 1H NMR (300 MHz, DMSO, δ ppm): 3.84 (s, 3H); 5.87 (s, 1H); 6.83 (s, 2H); 7.06 (d, *J* = 6.18 Hz, 2H); 7.42-7.49 (m, 3H); 7.81-7.87 (m, 4H); 7.92 (d, *J* = 5.85 Hz, 2H). MS (ESI): 320.41 ($[M+H]^+$). Anal. Calcd for $C_{19}H_{17}N_3O_2$: C, 71.46; H, 5.37; N, 13.16%; Found: C, 71.63; H, 5.44; N, 13.34%.

4.4.8 (*E*)-3-(4-bromophenyl)-*N*-(5-phenyl-1*H*-pyrazol-3-yl)acrylamide(5h)

Yellow powder, yield: 58%. m.p. 209-210 °C. 1H NMR (300 MHz, DMSO, δ ppm): 5.88 (s, 1H); 6.85 (s, 2H); 7.46 (m, 3H); 7.70 (d, *J* = 6.36 Hz, 2H); 7.81-7.93 (m, 5H); 7.99 (d, *J* = 12.09 Hz, 1H). MS (ESI): 369.32 ($[M+H]^+$). Anal. Calcd for $C_{18}H_{14}BrN_3O$: C, 58.71; H, 3.83; N, 11.41%; Found: C, 58.61; H, 3.76; N, 11.67%.

4.4.9 (*E*)-*N*-(5-(4-bromophenyl)-1*H*-pyrazol-3-yl)-3-(4-nitrophenyl)acrylamide (5i)

Yellow powder, yield: 55%. m.p. 230-231 °C. 1H NMR (300 MHz, DMSO, δ ppm): 5.91 (s, 1H); 6.91 (s. 2H); 7.67 (d, *J* = 6.36 Hz, 2H); 7.90 (d, *J* = 6.39 Hz, 2H); 7.99 (d, *J* = 12.12 Hz, 1H); 8.13 (m, 3H); 8.32 (d, *J* = 6.57 Hz, 2H). MS (ESI): 414.22 ($[M+H]^+$). Anal. Calcd for $C_{18}H_{13}BrN_4O_3$: C, 52.32; H, 3.17; N, 13.56%; Found: C, 52.49; H, 3.22; N, 13.79%.

4.4.10 (*E*)-*N*-(5-(4-bromophenyl)-1*H*-pyrazol-3-yl)-3-(4-(trifluoromethyl)phenyl)acrylamide(5j)

Yellow powder, yield: 82%. m.p. 180-181 °C. 1H NMR (300 MHz, DMSO, δ ppm): 5.90 (s, 1H); 6.91 (s, 2H); 7.66 (d, *J* = 6.33 Hz, 2H); 7.87 (m, 4H); 7.95-8.09 (m, 4H). MS (ESI): 437.62 ($[M+H]^+$). Anal. Calcd for $C_{19}H_{13}BrF_3N_3O$: C, 52.31; H, 3.00; N, 9.63%; Found: C, 52.49; H, 2.77; N, 9.58%.

4.4.11 *N*-(5-(4-bromophenyl)-1*H*-pyrazol-3-yl)cinnamamide(5k)

Yellow powder, yield: 65%. m.p. 215-216 °C. 1H NMR (300 MHz, DMSO, δ ppm): 5.90 (s, 1H); 6.89 (s, 2H); 7.51 (t, *J* =4.74, 3H); 7.66 (d, *J* = 6.39 Hz, 2H); 7.84-8.00 (m, 6H). MS (ESI): 369.11 ($[M+H]^+$). Anal. Calcd for $C_{18}H_{14}BrN_3O$: C, 58.71; H, 3.83; N, 11.41%; Found: C, 58.49; H, 3.65; N, 11.14%.

4.4.12 (*Z*)-*N*-(5-(4-bromophenyl)-1*H*-pyrazol-3-yl)-3-(4-fluorophenyl)acrylamide(5l)

Yellow powder, yield: 75%. m.p. 199-200 °C. 1H NMR (300 MHz, DMSO, δ ppm): 5.89 (s, 1H); 6.89 (s, 2H); 7.32-7.36 (m, 2H); 7.65 (d, *J* = 6.33 Hz, 2H); 7.88-7.96 (m, 6H). MS (ESI): 387.34 ($[M+H]^+$). Anal. Calcd for $C_{18}H_{13}BrFN_3O$: C, 55.98; H, 3.39; N, 10.88%; Found: C, 55.79; H, 3.22; N, 10.77%.

4.4.13 (*E*)-*N*-(5-(4-bromophenyl)-1*H*-pyrazol-3-yl)-3-(4-chlorophenyl)acrylamide(5m)

Yellow powder, yield: 66%. m.p. 179-180 °C. 1H NMR (300 MHz, DMSO, δ ppm): 5.89 (s, 1H); 6.88 (s, 2H); 7.49 (d, *J* = 5.55 Hz, 1H); 7.57 (d, *J* = 6.36 Hz, 2H); 7.66 (d, *J* = 6.39 Hz, 2H); 7.90 (m, 5H). MS (ESI): 403.57 ($[M+H]^+$). Anal. Calcd for $C_{18}H_{13}BrClN_3O$: C, 53.69; H, 3.25; N, 10.44%; Found: C, 53.47; H, 3.43; N, 10.57%.

4.4.14 (*E*)-*N*-(5-(4-bromophenyl)-1*H*-pyrazol-3-yl)-3-(*p*-tolyl)acrylamide(5n)

Yellow powder, yield: 36%. m.p. 213-214 °C. 1H NMR (300 MHz, DMSO, δ ppm): 2.38 (s, 3H); 5.89 (s, 1H); 6.87 (s, 2H); 7.33 (d, *J* = 5.91 Hz, 2H); 7.66 (d, J =

6.39 Hz, 2H); 7.75 (d, *J* = 6.09 Hz, 2H); 7.89 (m, 4H). MS (ESI): 383.19 ([M+H]+). Anal. Calcd for $C_{19}H_{16}BrN_3O_2$: C, 57.30; H, 4.05; N, 10.55%; Found: C, 57.21; H, 4.09; N, 10.32%.

4.4.15 (*E*)-*N*-(5-(4-bromophenyl)-1*H*-pyrazol-3-yl)-3-(4-methoxyphenyl)acrylamide(5o)

Yellow powder, yield: 65%. m.p. 185-186 °C. 1H NMR (300 MHz, DMSO, δ ppm): 3.85 (s, 3H); 5.88 (s, 1H); 6.86 (s, 2H); 7.06 (d, *J* = 6.57 Hz, 2H); 7.65 (d, *J* = 6.36 Hz, 2H); 7.84 (m, 6H). MS (ESI): 399.23 ($[M+H]^+$). Anal. Calcd for $C_{19}H_{16}BrN_3O_2$: C, 57.30; H, 4.05; N, 10.55%; Found: C, 57.49; H, 4.22; N, 10.77%.

4.4.16 (*E*)-3-(4-bromophenyl)-*N*-(5-(4-bromophenyl)-1*H*-pyrazol-3-yl)acrylamide (5p)

Yellow powder, yield: 65%. m.p. 186-187 °C. 1H NMR (300 MHz, DMSO, δ ppm): 5.90 (s, 1H); 6.88 (s, 2H); 7.65 (m, 4H); 7.71 (d, *J* = 6.36 Hz, 3H); 7.82 (d, *J* = 6.39 Hz, 2H); 7.98 (d, *J* = 6.09 Hz, 1H). MS (ESI): 448.41 ($[M+H]^+$). Anal. Calcd for $C_{18}H_{13}Br_2N_3O$: C, 48.35; H, 2.93; N, 9.40%; Found: C, 48.54; H, 2.65; N, 9.14%.

4.4.17 (*E*)-3-(4-nitrophenyl)-*N*-(5-(p-tolyl)-1*H*-pyrazol-3-yl)acrylamide(5q)

Yellow powder, yield: 54%. m.p. 209-210 °C. 1H NMR (300 MHz, DMSO, δ ppm): 2.36 (s, 3H); 5.86 (s, 1H); 6.86 (s, 2H); 7.28 (d, *J* = 5.97 Hz, 2H); 7.82 (d, *J* = 6.09 Hz, 2H); 7.98-8.15 (m, 4H); 8.32 (d, *J* = 6.57 Hz, 2H). MS (ESI): 349.35 ($[M+H]^+$). Anal. Calcd for $C_{19}H_{16}N_4O_3$: C, 65.51; H, 4.63; N, 16.08%; Found: C, 66.49; H, 4.47; N, 16.32%.

4.4.18 (*E*)-*N*-(5-(*p*-tolyl)-1*H*-pyrazol-3-yl)-3-(4-(trifluoromethyl)phenyl)acrylamide(5r)

Yellow powder, yield: 78%. m.p. 171-172 °C. 1H NMR (300 MHz, DMSO, δ ppm): 2.36 (s, 3H); 5.85 (s, 1H); 6.85 (s, 2H); 7.28 (d, *J* = 6.06 Hz, 2H); 7.83 (m, 4H); 8.03 (m, 4H). MS (ESI): 372.44 ($[M+H]^+$). Anal. Calcd for $C_{20}H_{16}F_3N_3O$: C, 64.69; H, 4.34; N, 11.32%; Found: C, 64.79; H, 4.47; N, 11.48%.

4.4.19 *N*-(5-(*p*-tolyl)-1*H*-pyrazol-3-yl)cinnamamide(5s)

Yellow powder, yield: 69%. m.p. 196-197 °C. 1H NMR (300 MHz, DMSO, δ ppm): 2.36 (s, 3H); 5.85 (s, 1H); 6.83 (s, 2H); 7.27 (d, *J* = 5.94 Hz, 2H); 7.50 (t, *J* = 4.71 Hz, 3H); 7.8-8.0 (m, 6H). MS (ESI): 304.52 ($[M+H]^+$). Anal. Calcd for $C_{19}H_{17}N_3O$: C, 75.23; H, 5.65; N, 13.85%; Found: C, 75.47; H, 5.77; N, 13.56%.

4.4.20 (*E*)-3-(4-fluorophenyl)-*N*-(5-(*p*-tolyl)-1*H*-pyrazol-3-yl)acrylamide(5t)

Yellow powder, yield: 65%. m.p. 186-187 °C. 1H NMR (300 MHz, DMSO, δ ppm): 2.36 (s, 3H); 5.84 (s, 1H); 6.82 (s, 2H); 7.31 (m, 4H); 7.80-7.96 (m, 6H). MS (ESI): 322.63 ($[M+H]^+$). Anal. Calcd for $C_{19}H_{16}FN_3O$: C, 71.01; H, 5.02; N, 13.08%; Found: C, 69.94; H, 5.65; N, 11.14%.

4.4.21 (*E*)-3-(4-chlorophenyl)-*N*-(5-(*p*-tolyl)-1*H*-pyrazol-3-yl)acrylamide(5u)

Yellow powder, yield: 65%. m.p. 180-181 °C. 1H NMR (300 MHz, DMSO, δ ppm): 2.36 (s, 3H); 5.84 (s, 1H); 6.83 (s, 2H); 7.27 (d, *J* = 6.00 Hz, 2H); 7.56 (d, *J* = 6.36 Hz, 2H); 7.81 (d, *J* = 6.06 Hz, 2H); 7.94 (m, 4H). MS (ESI): 338.86 ($[M+H]^+$). Anal. Calcd for $C_{19}H_{16}ClN_3O$: C, 67.56; H, 4.77; N, 12.44%; Found: C, 66.79; H, 4.52; N, 12.78%.

4.4.22 (*E*)-3-(*p*-tolyl)-*N*-(5-(*p*-tolyl)-1*H*-pyrazol-3-yl)acrylamide(5v)

Yellow powder, yield: 66%. m.p. 143-144 °C. 1H NMR (300 MHz, DMSO, δ ppm): 2.37 (d, *J* = 6.06 Hz, 2H); 5.84 (s, 1H); 6.82 (s, 2H); 7.27 (d, *J* = 6.00 Hz, 2H); 7.32 (d, *J* = 5.91 Hz, 2H); 7.74 (d, *J* = 6.00 Hz, 2H); 7.81 (d, *J* = 6.03 Hz, 2H); 7.90 (d, *J* = 6.15 Hz, 2H). MS (ESI): 318.12 ($[M+H]^+$). Anal. Calcd for $C_{19}H_{16}BrN_3O_2$: C, 75.69; H, 6.03; N, 13.24%; Found: C, 74.21; H, 6.09; N, 13.32%.

4.4.23 (*E*)-3-(4-methoxyphenyl)-*N*-(5-(*p*-tolyl)-1*H*-pyrazol-3-yl)acrylamide(5w)

Yellow powder, yield: 69%. m.p. 166-167 °C. 1H NMR (300 MHz, DMSO, δ ppm): 2.36 (s, 3H); 3.84 (s, 3H); 5.83 (s, 1H); 6.81 (s, 2H); 7.06 (d, *J* = 6.60 Hz, 2H); 7.27 (d, *J* = 5.94 Hz, 2H); 7.84 (m, 6H). MS (ESI): 334.23 ($[M+H]^+$). Anal. Calcd for $C_{20}H_{19}N_3O_2$: C, 72.05; H, 5.74; N, 12.60%; Found: C, 72.23; H, 5.54; N, 12.34%.

4.4.24 (*E*)-3-(4-bromophenyl)-*N*-(5-(*p*-tolyl)-1*H*-pyrazol-3-yl)acrylamide(5x)

Yellow powder, yield: 78%. m.p. 187-188 °C. 1H NMR (300 MHz, DMSO, δ ppm): 2.36 (s, 3H); 5.84 (s, 1H); 6.83 (s, 2H); 7.27 (d, *J* = 5.94 Hz, 2H); 7.70 (d, *J* = 6.36 Hz, 2H); 7.85 (m, 5H); 7.99 (d, *J* = 12.06 Hz, 1H). MS (ESI): 383.38 ($[M+H]^+$). Anal. Calcd for $C_{19}H_{16}BrN_3O$: C, 59.70; H, 4.22; N, 10.99%; Found: C, 59.56; H, 4.35; N, 10.78%.

4.5.Antiproliferation activity

The antiproliferative activities of the prepared compounds against MCF-7, A549

and B16-F10 cells was evaluated as described elsewhere with some modifications.[17] Target tumor cell line was grown to log phase in RPMI 1640 medium supplemented with 10% fetal bovine serum. After diluting to 2×10^4 cells/mL with the complete medium, 100 μL of the obtained cell suspension was added to each well of 96-well culture plates. The subsequent incubation was permitted at 37 ^oC, 5% CO_2 atmosphere for 24 h before the cytotoxicity assessments. Tested samples at pre-set concentrations were added to 6 wells with colchicine and CSA-4 coassayed as positive reference. After 48 h exposure period,40 μL of PBS containing 2.5 mg/mL of MTT (3-(4,5-dimethylthiazol-2-yl)-2,5-diphenyltetrazolium bromide)) was added to each well. Four hours later, 100 μL extraction solution (10% SDS-5% isobutyl alcohol-0.01M HCl) was added. After an overnight incubation at 37 ^oC, the optical density was measured at a wavelength of 570 nm on an ELISA microplate reader. In all experiments three replicate wells were used for each drug concentration. Each assay was carried out for at least three times. The results were summarized in Table 1.

4.6.Effects on tubulin polymerization

Bovine brain tubulin was purified as described previously.[31] To evaluate the effect of the compounds on tubulin assembly in vitro,[32] varying concentrations were preincubated with 10 μM tubulin in glutamate buffer at 30 ℃ and then cooled to 0 ℃. After addition of GTP, the mixtures were transferred to 0 ℃ cuvettes in a recording spectrophotometer and warmed up to 30 ℃ and the assembly of tubulin was observed turbidimetrically. The IC_{50} was defined as the compound concentration that inhibited the extent of assembly by 50% after 20 min incubation. In all experiments three replicate wells were used for each drug concentration. The results were summarized in Table 2.

4.7.Docking simulations

The crystal structures of tubulin (PDB code: 1SA0) was obtained from the Protein Data Bank (http://www.rcsb.org). Molecular docking of compound **5j** into the three-dimensional X-ray structure of tubulin was carried out using CDOCKER Dock

protocol of Discovery Studio 3.5. All bound water and ligands were eliminated from the protein and the polar hydrogen was added. The whole tubulin complex was defined as a receptor and the site sphere was selected based on the ligand binding location of colchicine, then the colchicine molecule was removed and **5j** was placed during the molecular docking procedure. Types of interactions of the docked protein with ligand were analyzed after the end of molecular docking.

4.8.QSAR model

79% (that is 19) of the compound were utilized as a training set for QSAR modeling and the remaining 21% (that is 5) were chosen as an external test subset for validating the reliability of the QSAR model by the Diverse Molecules protocol in Discovery Studio 3.5. The selected test compounds were: **5e**, **5h**, **5j**, **5m**, **5o**.

The inhibitory activities of the compounds in literatures [IC_{50} (mol/L)] was initially changed into the minus logarithmic scale [IC_{50} (mol/L)] and then used for subsequent QSAR analysis as the response variable.

In Discovery Studio, the CHARMm force field is used and the electrostatic potential and the van der Waals potential are treated as separate terms. A +1e point charge is used as the electrostatic potential probe and distance-dependent dielectric constant is used to mimic the solvation effect. For the van der Waals potential a carbon atom with a 1.73 Å radius is used as a probe.

A Partial Least-Squares (PLS) model is built using energy grids as descriptors. QSAR models were built by using the Create 3D QSAR Model protocol in Discovery Studio 3.5.

Acknowledgements

This work was supported by Natural Science Foundation of Jiangsu Province (No. BK20130554) and supported by Major Projects on Control and Rectification of Water Body Pollution (No. 2011ZX07204-001-2214 004).

References

[1]. G. Bacher, T. Beckers, P. Emig, T. Klenner, B. Kutscher, B. Nickel, Pure Appl. Chem. 73 (2001)1459-1464.

[2]. M. A. Jordan, L. Wilson, Nat. Rev. Cancer 4(2004),253-265.

[3]. A. Frace, C. Loge, S. Gallet, N. Lebegue, P. Carato, P. Chavatte, P. Berthelot, D. J. Lesieur, Enz. Inh. Med. Chem. 19(2004)541-547.

[4]. P. B.Schiff, J. Fant, S. B. Horwitz, Nature, 277(1979)665-667.

[5]. R. O. Carlson, Expert Opin. Investig. Drugs 17(2008)707-722.

[6]. E. Hamel, Med. Res. Rev. 16(1996)207-231.

[7]. R. B. Ravelli, B. Gigant, P. A. Curmi, I. Jourdain, S. Lachkar, A. Sobel, M. Knossow, Nature 428(2004)198-202.

[8]. J. Y. Chang, H. P. Hsieh, C. Y. Chang, K. S. Hsu, Y. F. Chiang, C. M. Chen, C. C. Kuo, J. P. Liou, J. Med. Chem. 49(2006)6656-6659.

[9]. M. L. Go, X. Wu, X. L. Liu, Curr. Med. Chem. 12(2005)481-499.

[10]. E. J. Park, H. R. Park, J. S. Lee, J. Kim, Planta Med. 64(1998)464-466.

[11]. A. C. Claude, C. L. Jean, T. Patric, P. Christelle, H. Gerard, J. C. Albert, L. D. Jean, Anticancer Res. 21(2001)3949-3956.

[12]. S. K. Kumar, H. Erin, P. Catherine, G. Halluru, N. E. Davidson, S. R. Khan, J. Med. Chem. 46(2003)2813-2815.

[13]. H. H. Ko, L. T. Tsao, K. L. Yu, C. T. Liu, J. P. Wang, C. N. Lin, Bioorg. Med. Chem. 11(2003)105-111.

[14]. F. Herencia, M. L. Ferrandiz, A. Ubeda, J. N. Dominguez, J. E. Charris, G. M. Lobo, M. J. Alcaraz, Bioorg. Med. Chem. Lett. 8(1998)1169-1174.

[15]. Y. M. Lin, Y. Zhou, M. T. Flavin, L. M. Zhou, W. Nie, F. C. Chen, Bioorg. Med. Chem. 10(2002)2795-2802.

[16]. K. L. Lahtchev, D. I. Batovska, St.P. Parushev, V. M. Ubiyvovk, A. A. Sibirny, Eur. J. Med. Chem. 43(2008)2220-2228.

[17]. A. Boumendjel, J. Boccard, P. A. Carrupt, E. Nicolle, M. Blanc, A. Geze, L. Choisnard, D. Wouessidjewe, E. L. Matera, C. Dumontet, J. Med. Chem. 51(2008)2307-2310.

[18]. M. Cabrera, M. Simoens, G. Falchi, M. L. Lavaggi, O. E. Piro, E. E.

Castellano, A. Vidal, A. Azqueta, A. Monge, A. Lopez de Cerain, G. Sagrera, G. Seoane, H. Cerecetto, M. Gonzalez, Bioorg. Med. Chem. 15(2007)3356-3367.

[19]. D. Y. Kim, K. H. Kim, N. D. Kim, K. Y. Lee, C. K. Han, J. H. Yoon, S. K. Moon, S. S. Lee, B. L. Seong, J. Med. Chem. 49(2006)5664-5670.

[20]. M. L. Go, X. Wu, X. L. Liu, Curr. Med. Chem. 12(2005)481-499.

[21]. D. J. Kerr, E. Hamel, M. K. Jung, B. L. Flynn, Bioorg. Med. Chem. 15(2007)3290-3298.

[22]. J. C. Jung, S. Jang, Y. Lee, D. Min, E. Lim, H. Jung, M. Oh, S. Oh, M. Jung, J. Med. Chem. 51(2008)4054-4058.

[23]. R. A. Stanton, K. M. Gernert, J. H. Nettles, R. Aneja, Medicinal Research Reviews 3(2011)443-481.

[24]. J. R. Dimmock, D. W. Elias, M. A. Beazely, N. M. Kandepu, Curr. Med. Chem. 6(1999)1125-1149.

[25]. P. De, M. Baltas, F. Bedos-Belval, Current medicinal chemistry. 11(2011)1672-1703.

[26]. Y. Qian, H. J. Zhang, H. Zhang, C. Xu, J. Zhao, H. L. Zhu, Bioorg. Med. Chem. 18(2010)4991-4996.

[27]. Y. Luo, K. M. Qiu, X. Lu, K. Liu, J. Fu, H. L. Zhu, Bioorg. Med. Chem. 19(2011)4730-4738.

[28]. X. H. Yang, Q. Wen, T. T. Zhao, J. Sun, X. Li, M. Xing, X. Lu, H. L. Zhu, Bioorg. Med. Chem. 20(2012)1181-1187.

[29]. R. Zaninetti, S. V. Cortese, S. Aprile, A. Massarotti, P. L. Canonico, G. Sorba, G. Grosa, A. A. Genazzani, T. Pirali, Chem. Med. Chem. 8(2013)633-643.

[30]. K. Ohsumi, T. Hatanaka, K. Fujiita, R. Nakagawa, Y. Fukuda, Y. Nihei, Y. Suga, Y. Morinaga, Y. Akiyama, T. Tsuji, Bioorg. Med. Chem. Lett. 8(1998)3153-3158.

[31]. E. Hamel, C. M. Lin, Biochemistry 23(1984)4173-4184.

[32]. E. Hamel, Cell Biochem. Biophys.38(2003)1-21.

Figure Captions

Table 1. Structural features, inhibition (IC_{50}) of MCF-7, A549 and B16-F10 cells proliferation by compounds **5a-5x**

Table 2. Tubulin inhibitory activities of synthetic compounds.

Table 3. Experimental, predicted inhibitory activities of compounds **5a-5x** by 3D-QSAR models based upon active conformation achieved by molecular docking.

Figure 1. Chemical structures of antimitotic agents and lead tubulin inhibitors.

Figure 2. Similar part of chalcone and cinnamon amide.

Figure 3. Effects of compound **5j** on cell cycle progression of MCF-7 cells were determined by flow cytometry analysis. MCF-7 cells were treated with different concentrations of **5j** for 24 h. The percentage of cells in each cycle phase was indicated.

Figure 4. Binding mode of compound **5j** with tubulin. For clarity, only interacting residues were labeled. Hydrogen bonding interactions are shown in dotted lines. This figure was made using Discovery Studio 3.5.

Figure 5. Binding mode of compound **5j** with tubulin. The enzyme is shown as surface; while **5j** docked structures are shown as sticks. This figure was made using Discovery Studio 3.5.

Figure 6. Plot of experimental versus predicted tubulin inhibitory activities of training set and test set.

Figure 7. (a) 3D-QSAR model coefficients on electrostatic potential grids. Blue represents positive coefficients; red represents negative coefficients. (b) 3D-QSAR model coefficients on van der Waals grids. Green represents positive coefficients; yellow represents negative coefficients.

Scheme 1. Synthesis of compounds **5a-5x**. Reagents and conditions: (a) CH_3CN, NaH, THF, reflux, 4 h; (b) $NH_2NH_2 \cdot H_2O$, CH_3SO_3H, EtOH, reflux, 1 h; (c) EDCl, HOBt, dichloromethane, reflux, 1 h.

Table 1. Structural features, inhibition (IC_{50}) of MCF-7, A549 and B16-F10 cells proliferation by compounds **5a**-**5x**

compound	R_1	R_2	**IC_{50}±SD (μM)**[a]		
			MCF-7[b]	A549[c]	B16-F10[d]
5a	H	4-NO_2	0.63±0.08	0.97±0.11	0.72±0.04
5b	H	4-CF_3	0.54±0.23	0.88±0.09	0.64±0.06
5c	H	H	1.36±0.34	1.58±0.14	1.56±0.17
5d	H	4-F	0.84±0.16	1.22±0.16	1.25±0.15
5e	H	4-Cl	0.97±0.24	1.39±0.24	1.27±0.34
5f	H	4-Me	1.78±0.18	1.77±0.21	1.68±0.36
5g	H	4-OMe	0.72±0.33	1.06±0.18	0.95±0.07
5h	H	4-Br	1.24±0.14	1.46±0.31	1.38±0.14
5i	Br	4-NO_2	0.56±0.22	0.74±0.24	0.63±0.09
5j	Br	4-CF_3	0.35±0.08	0.62±0.18	0.57±0.17
5k	Br	H	1.12±0.16	1.44±0.06	1.27±0.22
5l	Br	4-F	0.64±0.25	0.93±0.17	0.85±0.16
5m	Br	4-Cl	0.77±0.17	1.21±0.08	1.08±0.08
5n	Br	4-Me	1.17±0.06	1.62±0.05	1.48±0.09
5o	Br	4-OMe	0.59±0.08	0.82±0.22	0.77±0.16
5p	Br	4-Br	0.92±0.15	1.36±0.24	1.28±0.18
5q	CH_3	4-NO_2	0.84±0.09	1.13±0.16	1.32±0.27
5r	CH_3	4-CF_3	0.72±0.21	1.02±0.11	1.21±0.32
5s	CH_3	H	1.63±0.03	1.67±0.13	1.68±0.21
5t	CH_3	4-F	0.95±0.17	1.25±0.09	1.43±0.44
5u	CH_3	4-Cl	1.19±0.14	1.49±0.35	1.52±0.38
5v	CH_3	4-Me	1.72±0.25	1.88±0.33	1.75±0.34
5w	CH_3	4-OMe	0.86±0.07	1.19±0.41	1.37±0.25
5x	CH_3	4-Br	1.37±0.34	1.59±0.21	1.57±0.36
Colchicine			0.39±0.05	0.58±0.08	0.48±0.07
CA-4			0.21±0.06	0.46±0.04	0.42±0.06

[a] The averaged values determined by at least three separate determinations.

[b] Inhibition of the growth of MCF-7 cell lines.

[c] Inhibition of the growth of A549 cell lines.

[d] Inhibition of the growth of B16-F10 cell lines.

Table 2. Tubulin inhibitory activities of synthetic compounds.

compound	R_1	R_2	IC_{50}±SD(μM)[a]
5a	H	4-NO_2	1.56±0.21
5b	H	4-CF_3	1.34±0.34
5c	H	H	2.84±0.27
5d	H	4-F	1.85±0.22
5e	H	4-Cl	2.06±0.19
5f	H	4-Me	3.02±0.27
5g	H	4-OMe	1.64±0.15
5h	H	4-Br	2.36±0.24
5i	Br	4-NO_2	1.24±0.11
5j	Br	4-CF_3	1.02±0.09
5k	Br	H	2.55±0.26
5l	Br	4-F	1.78±0.18
5m	Br	4-Cl	1.95±0.22
5n	Br	4-Me	2.76±0.39
5o	Br	4-OMe	1.35±0.17
5p	Br	4-Br	2.14±0.33
5q	CH_3	4-NO_2	1.62±0.16
5r	CH_3	4-CF_3	1.53±0.18
5s	CH_3	H	3.12±0.29
5t	CH_3	4-F	1.92±0.28
5u	CH_3	4-Cl	2.15±0.44
5v	CH_3	4-Me	3.36±0.36
5w	CH_3	4-OMe	1.76±0.16
5x	CH_3	4-Br	2.55±0.35
Colchicine			1.34±0.23
CA-4			0.68±0.16

[a] The averaged values determined by three separate determinations.

Table 3. Experimental, predicted inhibitory activities of compounds **5a-5x** by 3D-QSAR models based upon active conformation achieved by molecular docking

compound [a]	tubulin		Residual error
	Actual pIC_{50}	Predicted pIC_{50}	
5a	5.807	5.845	-0.038
5b	5.873	5.888	-0.015
5c	5.547	5.633	-0.086
5d	5.733	5.757	-0.024
5e	5.686	5.690	-0.004
5f	5.52	5.523	-0.003
5g	5.785	5.763	0.022
5h	5.627	5.648	-0.021
5i	5.907	5.781	0.126
5j	5.991	5.962	0.029
5k	5.593	5.539	0.054
5l	5.75	5.712	0.038
5m	5.71	5.739	0.029
5n	5.56	5.519	0.041
5o	5.87	5.817	0.053
5p	5.67	5.696	-0.026
5q	5.79	5.790	0.000
5r	5.815	5.816	-0.001
5s	5.506	5.555	-0.049
5t	5.717	5.687	0.030
5u	5.668	5.717	-0.049
5v	5.474	5.467	0.007
5w	5.754	5.760	-0.006
5x	5.593	5.623	-0.030

[a] Underlined compounds were selected as the test sets while the rest ones were in the training sets.

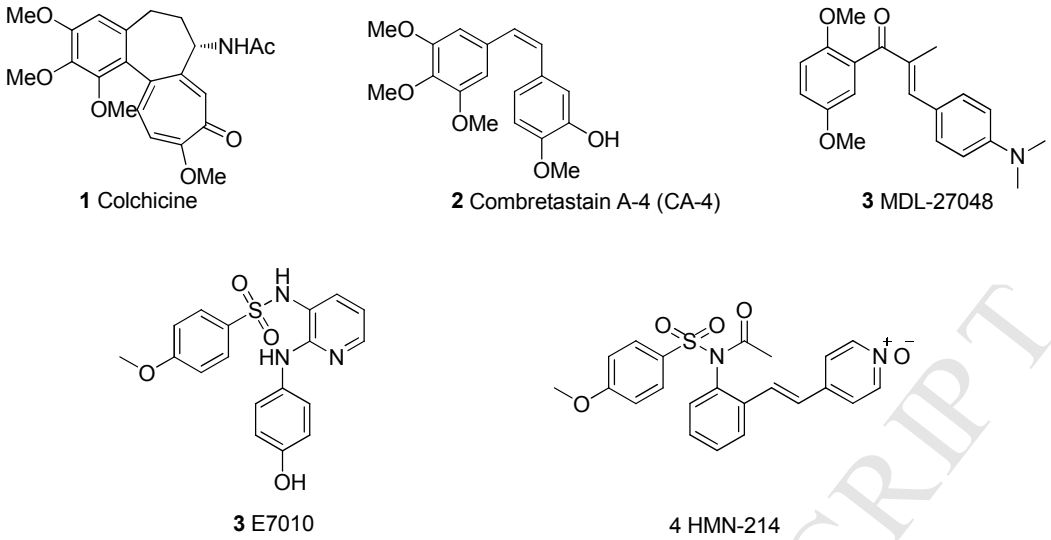

Figure 1. Chemical structures of antimitotic agents and lead tubulin inhibitors.

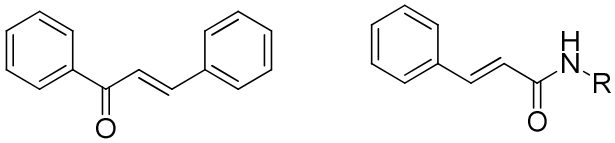

Figure 2. Similar part of chalcone and cinnamon amide.

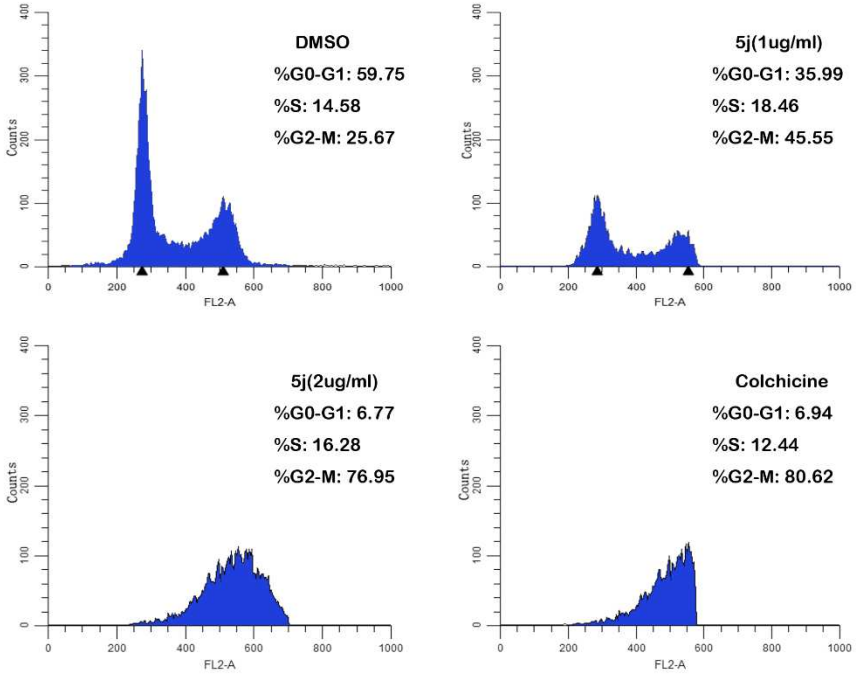

Figure 3. Effects of compound **5j** on cell cycle progression of MCF-7 cells were determined by flow cytometry analysis. MCF-7 cells were treated with different concentrations of **5j** for 24 h. The percentage of cells in each cycle phase was indicated.

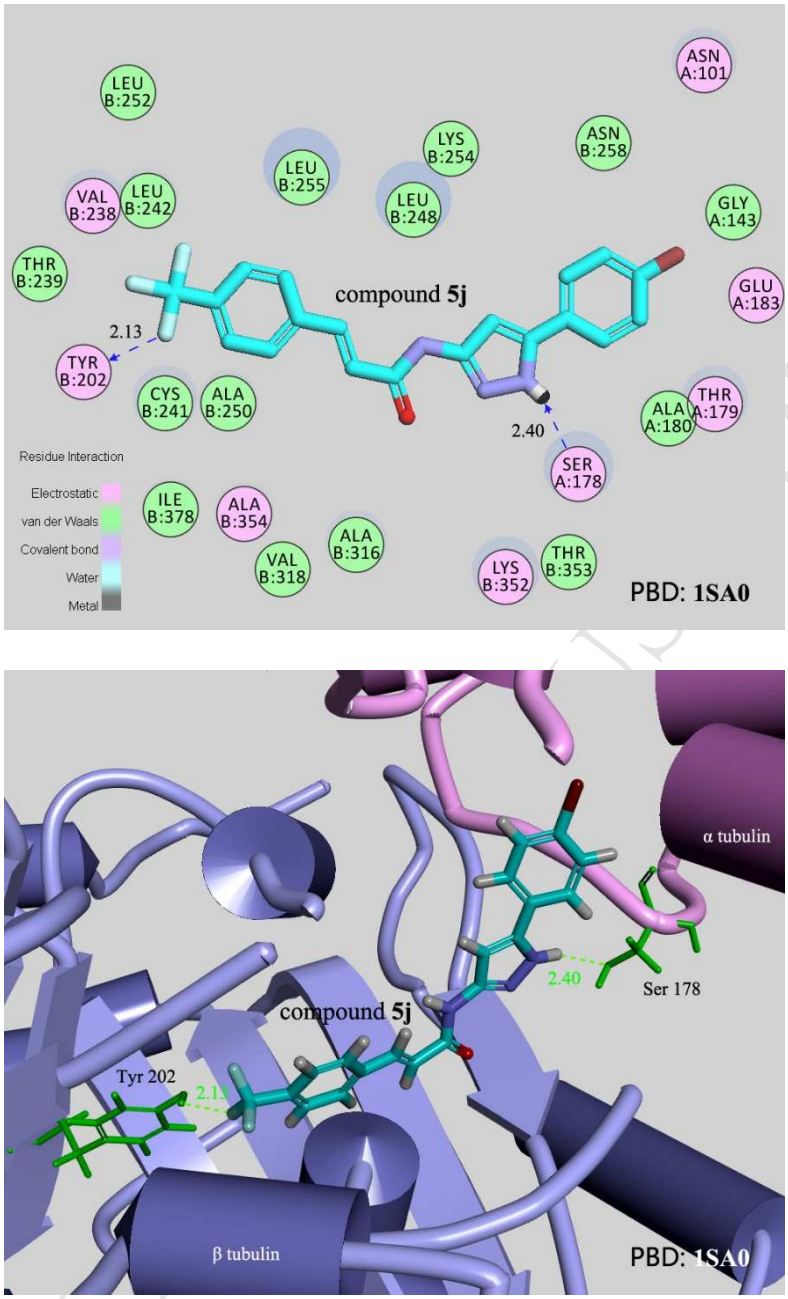

Figure 4. Binding mode of compound **5j** with tubulin. For clarity, only interacting residues were labeled. Hydrogen bonding interactions are shown in dotted lines. This figure was made using Discovery Studio 3.5.

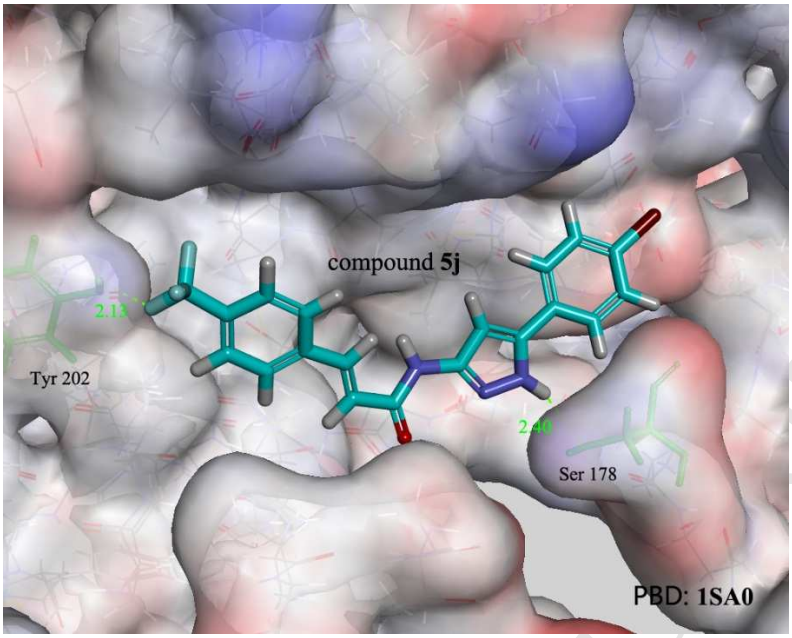

Figure 5. Binding mode of compound **5j** with tubulin. The enzyme is shown as surface; while **5j** docked structures are shown as sticks. This figure was made using Discovery Studio 3.5.

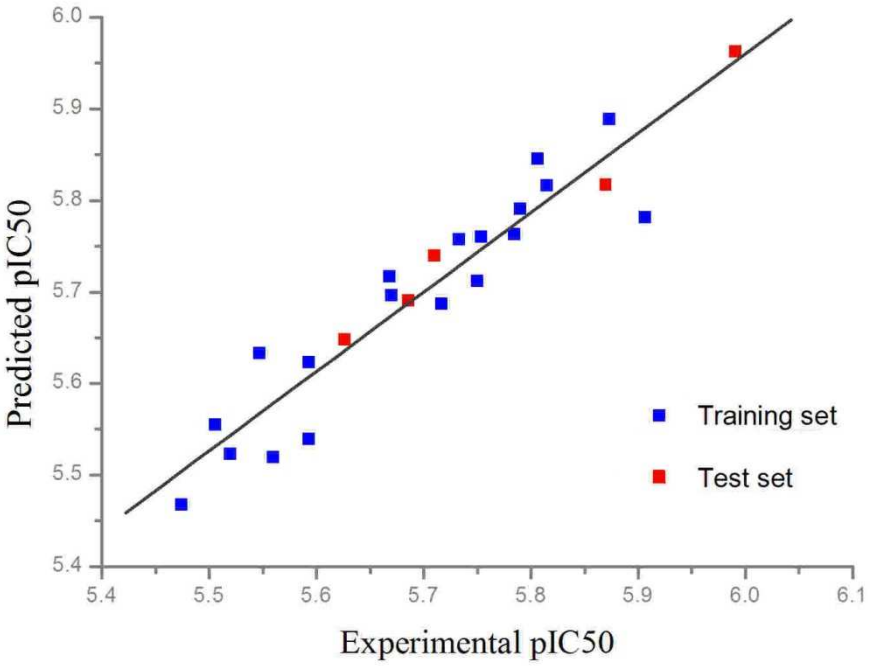

Figure 6. Plot of experimental versus predicted tubulin inhibitory activities of training set and test set.

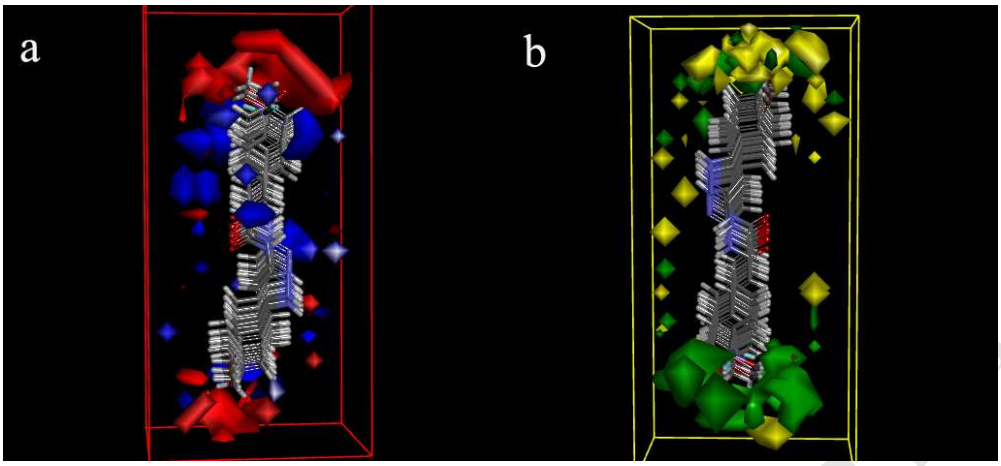

Figure 7. (a) 3D-QSAR model coefficients on electrostatic potential grids. Blue represents positive coefficients; red represents negative coefficients. (b) 3D-QSAR model coefficients on van der Waals grids. Green represents positive coefficients; yellow represents negative coefficients.

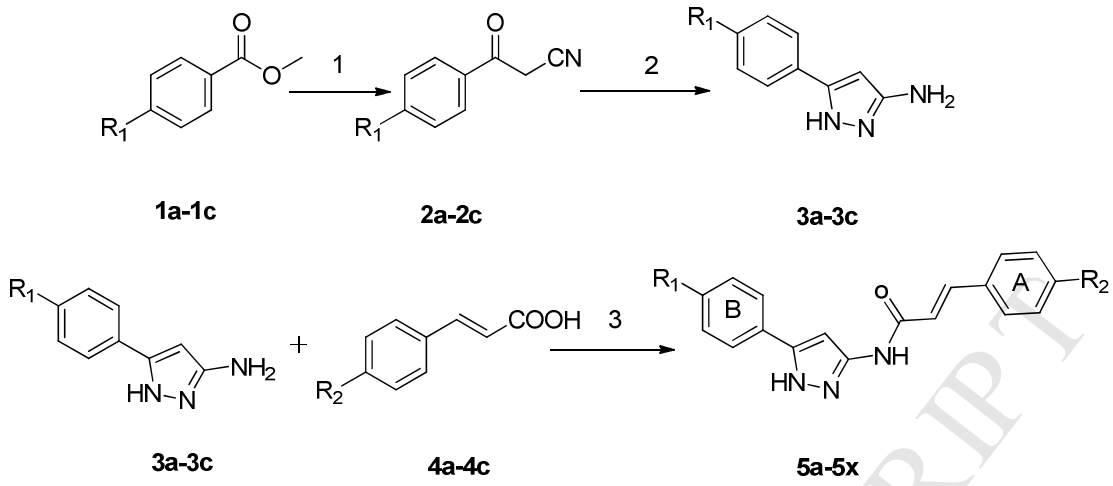

Scheme 1. Synthesis of compounds **5a**-**5x**. Reagents and conditions: (1) CH_3CN, NaH, THF, reflux, 4 h; (2) $NH_2NH_2 \cdot H_2O$, CH_3SO_3H, EtOH, reflux, 1 h; (3) EDCl, HOBt, dichloromethane, reflux, 1 h.

- 24 novel 5-phenyl-1*H*-pyrazol cinnamamide derivatives had been synthesized.
- The compounds were evaluated for biological activities as tubulin inhibitors.
- Compound **5j** showed the most potent inhibitory activity.